THE JOURNAL OF BIOLOGICAL CHEMISTRY VOL. 290, NO. 31, pp. 19184–19196, July 31, 2015

Chitoporin from the Marine Bacterium *Vibrio harveyi*

*PROBING THE ESSENTIAL ROLES OF TRP[136] AT THE SURFACE OF THE CONSTRICTION ZONE**

Received for publication, April 21, 2015, and in revised form, June 2, 2015 Published, JBC Papers in Press, June 16, 2015, DOI 10.1074/jbc.M115.660530

Watcharin Chumjan[‡§1], Mathias Winterhalter[¶2], Albert Schulte[‡‖], Roland Benz[¶], and Wipa Suginta[‡§3]

From the [‡]Biochemistry-Electrochemistry Research Unit, the [§]School of Biochemistry, and the [‖]School of Chemistry, Suranaree University of Technology, Nakhon Ratchasima 30000, Thailand and the [¶]Department of Life Sciences and Chemistry, Jacobs University Bremen, D-28759 Bremen, Germany

Background: *Vh*ChiP is a sugar uptake channel specific for chitohexaose.
Results: Mutations of Trp[136], located at the entrance of the transmembrane pore, affect ion and sugar transport through *Vh*ChiP.
Conclusion: Trp[136] regulates chitooligosaccharide uptake through *Vh*ChiP.
Significance: Chitin uptake by the highly virulent bacterium *V. harveyi* through *Vh*ChiP is dependent on hydrophobic interactions between the sugar molecule and the channel surface.

***Vh*ChiP is a sugar-specific porin present in the outer membrane of the marine bacterium *Vibrio harveyi*. *Vh*ChiP is responsible for the uptake of chitin oligosaccharides, with particular selectivity for chitohexaose. In this study, we employed electrophysiological and biochemical approaches to demonstrate that Trp[136], located at the mouth of the *Vh*ChiP pore, plays an essential role in controlling the channel's ion conductivity, chitin affinity, and permeability. Kinetic analysis of sugar translocation obtained from single channel recordings indicated that the Trp[136] mutations W136A, W136D, W136R, and W136F considerably reduce the binding affinity of the protein channel for its best substrate, chitohexaose. Liposome swelling assays confirmed that the Trp[136] mutations decreased the rate of bulk chitohexaose permeation through the *Vh*ChiP channel. Notably, all of the mutants show increases in the off-rate for chitohexaose of up to 20-fold compared with that of the native channel. Furthermore, the cation/anion permeability ratio P_c/P_a is decreased in the W136R mutant and increased in the W136D mutant. This demonstrates that the negatively charged surface at the interior of the protein lumen preferentially attracts cationic species, leading to the cation selectivity of this trimeric channel.**

Vibrio harveyi, a Gram-negative bioluminescent marine bacterium of the family *Vibrionaceae*, causes *Vibriosis*, a highly virulent disease that has devastating effects on fish and prawn-farming industries worldwide (1–5). Through its ability to grow rapidly under both aerobic and anaerobic conditions, *V. harveyi* has a crucial role in the rapid turnover of chitin biomaterials in marine ecosystems. The pathway of chitin catabolism by *V. harveyi* involves chitin attachment and degradation, followed by chitooligosaccharide uptake through the bacterial outer and inner membranes and finally catabolism of the transport products, which are used as carbon and nitrogen sources and in cellular energy production (6–8).

Energy production in *V. harveyi* depends upon the generation of chitin degradation products and their transport into the cells. We recently identified chitoporin from *V. harveyi* (known as *Vh*ChiP) as a pore-forming channel that performs highly specific translocation of chitooligosaccharides (9, 10). Single channel recordings using a black lipid membrane (BLM)[4] reconstitution technique showed that *Vh*ChiP inserted into the artificial bilayer membranes and formed a trimeric channel that remained steadily open under applied potentials of up to ±150 mV. The fully open channel exhibited an average conductance of 1.8 ± 0.13 nS in 1 M KCl, which is much larger than the average conductance of maltoporin (also called LamB) (0.15 nS in 1 M KCl) from *Escherichia coli* (11).

Time-resolved single channel recordings and liposome swelling assays in the presence of various oligosaccharides showed that the *Vh*ChiP channel responded specifically to chitooligosaccharides, the strength of interaction increasing with greater chain length. Detailed assessment of the kinetic parameters suggested that *Vh*ChiP was most active with chitohexaose, its binding constant of $K = 500{,}000\ \text{M}^{-1}$ being several orders of magnitude higher than that of its sugar-specific homologues, such as sucrose-specific porin, maltose-specific porin, glucose-inducible porin, and cyclodextrin-specific porin (12–19). According to these data, *Vh*ChiP is the most active sugar-specific porin reported to date. Further analysis of stochastic fluctuations of ion current through *Vh*ChiP in the pres-

* The authors declare that they have no conflicts of interest with the contents of this article.
[1] Supported by CHE-PhD-SW Scholarship Contract 60/2550 from the Commission of Higher Education, Ministry of University Affairs (Bangkok, Thailand). This author's 15-month research visit in Germany was supported through the Deutscher Akademischer Austausch Dienst.
[2] To whom correspondence may be addressed. E-mail: m.winterhalter@jacobs-university.de.
[3] Supported by Thailand Research Fund Basic Research Grant BRG578001 and Suranaree University of Technology Grants SUT1-102-57-36-18 and SUT1-102-56-12-30. To whom correspondence should be addressed: Suranaree University of Technology, Nakhon Ratchasima, Thailand 30000, E-mail: wipa@sut.ac.th.

[4] The abbreviations used are: BLM, black lipid membrane; nS, nanosiemens; LDAO, lauryldimethylamine oxide.

TABLE 1
Primers for site-directed mutagenesis
Underlined sequences indicate the mutated codons.

Mutation	Nucleotide sequence
Trp$^{136\,(WT)}$	
Forward	5′-ataccatggcgtcttacctaaagaaaag-3′ (NcoI)
Reverse	5′-aacctcgagttagaagtagtattcaacac-3′ (XhoI)
Trp^{136} → Ala	
Forward	5′-ggtctaggtgatgtttacgacgcaggtggtgctatcggtggtgc-3′
Reverse	5′-gcaccaccgatagcaccacctgcgtcgtaaacatcacctagacc-3′
Trp^{136} → Phe	
Forward	5′-ggtctaggcgatgtttacgactttggtggtgcgattggtggtgc-3′
Reverse	5′-gcaccaccaatcgcaccaccaaagtcgtaaacatcgcctagacc-3′
Trp^{136} → Asp	
Forward	5′-ggtctaggcgatgtttacgacgatggtggtgcgatctgtggtgc-3′
Reverse	5′-gcaccacagatcgcaccaccatcgtcgtaaacatcgcctagacc-3′
Trp^{136} → Arg	
Forward	5′-ggtctaggcgatgtttacgaccgtggtggtgcgatctgtggtgc-3′
Reverse	5′-gcaccacagatcgcaccaccacggtcgtaaacatcgcctagacc-3′

ence of chitohexaose indicated that the chitoporin had multiple binding sites for sugars and exploited interactions between bound sugar molecules to enhance sugar uptake (19).

We previously predicted the structure of *Vh*ChiP using the Swiss-Model Server (9) with *Comamonas acidovorans* Omp32 as structural template (20) and demonstrated that the *Vh*ChiP monomer had a barrel-like structure, consisting of 16 antiparallel β-strands, eight extracellular loops (referred to as loops L1–L8), and eight short turns located on the periplasmic side of the outer membrane. The longest extracellular loop (L3), containing 41 amino acids (Gly^{111}–Asn^{151}) and lying between strands β7 and β8, is known as a pore-confined loop and is responsible for the size selectivity of other sugar-specific porins, such as LamB and ScrY (21, 22), and general diffusion porins (23). Within the pore lumen of *Vh*ChiP, there are several aromatic residues, including Trp^{136}, Tyr^{134}, Tyr^{145}, Tyr^{118}, and Trp^{123}, aligned on one side of the pore. By analogy with LamB, such residues may play an important role in sugar-protein interactions. Among these, Trp^{136}, as part of loop L3, is the only residue protruding into the center of the *Vh*ChiP lumen and clearly covering the upper part of the constriction zone. Its prominent position is presumed to be important for the physiological properties of *Vh*ChiP. In this study, we carried out site-directed mutagenesis and then further employed a black lipid membrane reconstitution technique as well as protein fluorescence quenching and proteoliposome swelling assays to systematically address the functional roles of Trp^{136} in the ion conductivity, substrate binding affinity, and sugar permeability of *Vh*ChiP.

Experimental Procedures

Vectors and Bacterial Strains—A cDNA fragment of 1.1 kbp corresponding to the full-length ChiP gene of *V. harveyi* was cloned in the expression vector pET23d(+) (Novagen, MERCK Ltd., Bangkok, Thailand). *E. coli* host strain BL21(DE3) Omp8 Rosetta was genetically engineered to carry defective genes encoding the major outer membrane porins OmpA, OmpC, OmpF, and LamB, making it suitable for production of an exogenous porin (24, 25).

Construction of Recombinant Plasmids of VhChiP Mutants—The *VhChiP* gene, cloned into pET23d(+) expression vector, was suitable for expression at a high level in the porin-deficient *E. coli* strain, as specified. For site-directed mutagenesis, the construction of pET23d(+)/*Vh*ChiP was used as DNA template in a PCR-based strategy. Site-directed mutagenesis was carried out following the QuikChange site-directed mutagenesis protocol of Stratagene. Based on the primers shown in Table 1, the residue Trp^{136} was replaced by Ala, Phe, Asp, or Arg, generating four single mutants, namely W136A, W136F, W136D, and W136R, respectively. To verify that mutations were correct, the nucleotide sequences of the sense and antisense strands of the PCR fragment were determined by automated sequencing (First BASE Laboratories Sdn Bhn, Selangor Darul Ehsan, Malaysia).

Expression and Purification of VhChiP Variants—Recombinant wild-type *Vh*ChiP and the W136A/F/D/R mutants were expressed and purified, following the protocol originally described by Garavito and Rosenbusch (26). In brief, transformed cells were grown at 37 °C in Luria-Bertani (LB) liquid medium containing 100 μg·ml^{-1} ampicillin, 25 μg·ml^{-1} kanamycin, and 1% (w/v) glucose. At an A_{600} of 0.6–0.8, isopropyl β-D-thiogalactoside was added to a final concentration of 0.5 mM. Cell growth was continued for a further 6 h, and cells were then harvested by centrifugation at 4,500 × *g* at 4 °C for 20 min. The cell pellet was resuspended in a buffer containing 20 mM Tris-HCl, pH 8.0, 2.5 mM $MgCl_2$, 0.1 mM $CaCl_2$, 10 μg·ml^{-1} DNase I, and 10 μg·ml^{-1} RNase A. Cells were lysed by sonication on ice for 10 min (30% duty cycle; amplitude setting 20%) using a Sonopuls Ultrasonic homogenizer with a 6-mm diameter probe. The recombinant *Vh*ChiP was extracted with SDS, based on the method of Lugtenberg and Alphen (27). Briefly, 20% SDS stock solution was added into the lysed cell suspension to obtain a 2% (w/v) final concentration, followed by incubation at 50 °C for 1 h with gentle stirring and centrifugation at 40,000 × *g* at 4 °C for 60 min. Native and mutant *Vh*ChiP were extracted from the pellets, which were enriched in outer membranes, in two steps. In a pre-extraction step, the pellet was washed with 15 ml of 0.125% *n*-octylpolyoxyethylene in 20 mM phosphate buffer, pH 7.4 (ALEXIS Biochemicals, Lausen, Switzerland), homogenized with a Potter-Elvehjem homogenizer, incubated at 37 °C for 60 min, and then centrifuged at 100,000 × *g* and 4 °C for 40 min. In the second step, the pellet from centrifugation at 100,000 × *g* was resuspended in 10–15

ml of 3% (v/v) *n*-octylpolyoxyethylene in 20 mM phosphate buffer, pH 7.4, and then homogenized with a Potter-Elvehjem homogenizer and incubated at 37 °C for 60 min, followed by further centrifugation at 100,000 × *g* and 4 °C for 40 min. After exchange of the detergent with 0.2% (v/v) lauryldimethylamine oxide (LDAO) (Sigma-Aldrich) by thorough dialysis, the supernatant was subjected to ion exchange chromatography on a HiTrap Q HP prepacked column (5 × 1 ml), connected to an ÄKTA Prime plus FPLC system (GE Healthcare). Bound proteins were eluted with a linear gradient of 0–1 M KCl in 20 mM phosphate buffer, pH 7.4, containing 0.2% (v/v) LDAO. The purity of the eluted proteins was confirmed by SDS-PAGE. Fractions containing only *Vh*ChiP were pooled, and the protein concentration was determined using the Pierce BCA protein assay kit (Bio-Active Co., Ltd., Bangkok, Thailand).

Confirmation of VhChiP Expression by Immunoblotting—Immunoblotting was performed following the standard enhanced chemiluminescence (ECL) protocol. Purified *Vh*ChiP (5 μg) was resolved on a 10% polyacrylamide-SDS gel, and after electrophoresis, the protein was transferred to a nitrocellulose membrane using a Trans-Blot SD semidry electrophoretic transfer cell (Bio-Rad). Cross-reactivity of different porins was tested using specific antisera directed against *E. coli* OmpF, *E. coli* OmpN, and *V. harveyi* ChiP. Antibody-antigen interaction was detected with HRP-conjugated IgG, using the ECL method (Amersham Biosciences). Rabbit anti-*Vh*ChiP antiserum was prepared in our laboratory as described by Suginta *et al.* (9).

BLM Measurements of the VhChiP—Effects of mutation on channel conductance were assessed by single channel measurements of *Vh*ChiP reconstituted in lipid bilayers formed either by solvent-containing (painting) or by solvent-depleted (lowering and raising) techniques. BLM measurements using the solvent-containing technique were carried out following Schulte *et al.* (28). Briefly, the BLM setup included a patch clamp amplifier with a two-electrode bilayer head stage (PC-ONE Plus PC-ONE-50, Dagan Corp., Minneapolis, MN), a Faraday cage placed on a vibration-dampening table, an analog to digital converter, and software for computer-controlled operation (PULSE program, HEKA Elektronik, Lambrecht, Germany). In the BLM setup, a 1.5-ml Delrin cup with a 200-μm hole was fitted tightly into one of the two wells of a polymer bilayer chamber. The interior of the cup (*cis*) and the vacant well (*trans*) were filled with the electrolyte solution in which the two Ag/AgCl/1 M KCl reference electrodes, connected to the amplifier's head stage, were immersed. Routinely, the *trans* electrode was voltage-clamped with respect to the *cis* electrode, which was connected to the ground pin of the amplifier head stage. BLMs were formed by painting asolectin (soybean phospholipids from Sigma-Aldrich, dissolved in hexane, at 50 mg·ml^{-1}) over a cup aperture that had been pretreated with 10 μl of hexadecane/hexane (1:100, v/v) and allowed to dry for 10 min. After formation of a membrane of about 100-picofarad capacitance, 10–20 μl of a stock solution of the purified *Vh*ChiP (100 ng·ml^{-1} in 20 mM phosphate buffer, pH 7.5, and 0.2% (v/v) LDAO) was added into the *cis* chamber. The buffer solution contained 1 M KCl on both sides of the BLM chamber, unless otherwise indicated. *Vh*ChiP insertions were initiated by applying an external transmembrane potential of ±200 mV. Membrane current (I_m) recordings were made at 25°C with the membrane potential across the phospholipid bilayer kept at defined constant values between −100 and +100 mV. The acquired data were filtered with a 3-pole low pass Bessel filter at 1 kHz and saved into the computer memory with a 1-ms (1-kHz) sampling interval. Current flow was analyzed directly with PULSE acquisition software, or stored traces were handled with Microsoft Office Excel 2007 and GraphPad Prism version 5.0 (GraphPad Software Inc., San Diego, CA).

The protocol for formation of solvent-depleted bilayers was slightly different (29–31). Briefly, the cuvette consisted of two chambers separated by a 25-μm-thick Teflon film. An aperture of 60–100-μm diameter was pretreated with 5 μl of 1% (v/v) hexadecane in hexane (Sigma-Aldrich) and dried for 10 min. To each side of the chamber was added 2.5 ml of 1 M KCl in 20 mM HEPES, pH 7.5, as electrolyte solution, and Ag/AgCl electrodes were inserted on either side of the Teflon film. Then 2–5 μl of 5 mg·ml^{-1} 1,2-diphytanoyl-*sn*-glycero-3-phosphatidylcholine; Avanti Polar Lipids, Alabaster, AL) in *n*-pentane was added to each side of the chamber and allowed to diffuse for 5–10 min. The lipid bilayer was formed by raising and lowering the liquid level on either side of the chamber repeatedly until the current fell to zero. The seal was checked by applying a potential of 200 mV, which should produce zero current. *Vh*ChiP (50–100 μg) was then added to the *cis* side of the lipid membrane. At applied transmembrane potentials of ±199 mV, a single channel was usually inserted within a few min. To prevent multiple insertions, the protein concentration in the chamber was gradually reduced by multiple additions of the working electrolyte. One of the electrodes (*cis*) was used as ground, whereas the other (*trans*) was connected to the head stage. Single channel current measurements were performed with an Axopatch 200B amplifier (Molecular Devices, Sunnyvale, CA) in the voltage clamp mode, with the internal filter set at 10 kHz. Amplitude, probability, and single channel analyses were performed using pClamp version 10.0 software (all from Molecular Devices, Sunnyvale, CA). To investigate sugar binding, different concentrations of chitohexaose (0.25, 1.25, 2.5, 5, and 10 μM) were added to either the *cis* or the *trans* side of the chamber (29–30). Occlusions of ion flow observed as a result of sugar binding/diffusion through the reconstituted channel were usually recorded for at least 60 s at transmembrane potentials of ±50 and ±100 mV.

The equilibrium binding constant K (M^{-1}) was estimated from the decrease in the ion conductance in the presence of increasing concentrations of sugar using the following equation (30, 32),

$$G_{max} - G_c/G_{max} = I_{max} - I_c/I_{max} = K(c)/(K(c) + 1) \quad \text{(Eq. 1)}$$

where G_{max} is the average conductance of the fully open *Vh*ChiP channel, and G_c is the average conductance at a given concentration (c) of a chitooligosaccharide. I_{max} is the initial current through the fully open channel in the absence of sugar, and I_c is the current at a particular sugar concentration. The titration experiments could also be analyzed using double reciprocal plots.

The association and dissociation rates of the sugar molecules to and from the binding site inside *Vh*ChiP were obtained using single channel analysis. For example, the off-rate k_{off} (s^{-1}) was obtained according to Kullman *et al.* (33).

$$k_{off} = 1/\tau_c \quad \text{(Eq. 2)}$$

Here τ_c is the residence (dwell) time (s) (*i.e.* the average time for which a sugar molecule remains in the channel). The on-rate (k_{on}, in $M^{-1}\cdot s^{-1}$) is given by the following.

$$k_{on} = K \cdot k_{off} \quad \text{(Eq. 3)}$$

In further experiments, single channels inserted in planar lipid membranes were used to study the ionic selectivity of the wild-type *Vh*ChiP and its mutants. The ion selectivity was evaluated by measuring the zero current membrane potential (V_m), defined as the transmembrane voltage that has to be applied to yield zero current in the presence of a concentration gradient across the channel. Lipid bilayer membranes were formed at salt concentration gradients starting from 0.1 M KCl on both sides, using the protocol for solvent-depleted membranes. *Vh*ChiP or its mutants were then reconstituted using high potentials (±150 or ±199 mV). The channel conductance was checked by applying different voltages. The salt concentration on the *trans* side (c') of the membranes was increased by adding 200 μl of 3 M KCl while the KCl concentration on the *cis* side (c'') was kept constant at 0.1 M. V_m was measured when the KCl concentration on the trans side (c') reached 1.5 M. The P_c/P_a values are the permeability ratios of cation over anion, which were calculated from the zero current potential using the Goldman-Hodgkin-Katz equation.

$$V_m = \frac{RT}{F} \ln \frac{P_c[K^+]^{cis} + P_a[Cl^-]^{trans}}{P_c[K^+]^{trans} + P_a[Cl^-]^{cis}} \quad \text{(Eq. 4)}$$

Here V_m is the membrane potential (V); R is the ideal gas constant (8.314 $J\cdot K^{-1}\cdot mol^{-1}$); T is the absolute temperature; F is Faraday's constant; P_c is the permeability for K^+; and P_a is the permeability for Cl^-.

Binding Studies Using Fluorescence Quenching—The purified *Vh*ChiP (80 ng·μl^{-1}, in 20 mM phosphate buffer, pH 7.4 and 0.2% (v/v) LDAO) was titrated with chitooligosaccharide at 25 ± 3 °C. Changes in intrinsic tryptophan fluorescence intensity were monitored directly with a LS-50 fluorescence spectrometer (PerkinElmer Life Sciences). The excitation wavelength was set to 295 nm, and emission spectra were collected over the range 300–550 nm, with excitation and emission slit widths of 5 and 10 nm, respectively. Each protein spectrum was corrected for the buffer. Binding curves were evaluated with a nonlinear regression function available in Prism version 5.0 (GraphPad Software) using a model based on a single binding site. To estimate the dissociation constant, relative fluorescence $\Delta F = (F_0 - F_c)$ was plotted as a function of sugar concentration, yielding a rectangular hyperbolic curve. This curve allowed the calculation of the dissociation constant for the chitooligosaccharide using a single site binding model, according to Equation 5 (34–36),

$$\Delta F = F_0 - F_c = (F_0 - F_{min})K(c)/(1 + K(c)) \quad \text{(Eq. 5)}$$

where ΔF is the difference between fluorescence intensity before and after addition of the sugar ligand; F_0 refers to the maximum emission intensity in the absence of sugar; F_{min} is the minimum emission intensity; F_c is the emission intensity at a given concentration of ligand; c is the concentration of ligand; and K is the equilibrium binding constant (M).

Liposome Swelling Assays—Liposome swelling assays were carried out to verify the permeability of *Vh*ChiP wild type (WT) and its mutants to chitohexaose (9, 37). *E. coli* total lipid extract (Avanti) (20 mg·ml^{-1} in chloroform) was used to form multilamellar liposomes and 17% (w/v) dextran (M_r 40,000) prepared in 20 mM HEPES buffer, pH 7.5, was entrapped in the liposomes. The purified WT *Vh*ChiP (100 ng) or its mutants were reconstituted into liposomes (9, 37). The isotonic solute concentration of each preparation of proteoliposomes was determined by adding 30 μl of D-raffinose solution, dissolved in 20 mM HEPES buffer, pH 7.5, at various concentrations (40, 50, 60, 70, and 80 mM) into 600 μl of the proteoliposome suspension in a 1-ml cuvette and mixed manually. Changes in apparent absorbance at 500 nm (A_{500}) were followed for 60 s using a UV-visible spectrophotometer. The final concentration of D-raffinose that yielded an absorbance change of <0.01 was considered to be the isotonic concentration, which was then used to prepare different isotonic solute solutions. To measure the swelling rate, the liposome or proteoliposome suspension was diluted with the isotonic test solution as described above. The concentration of chitohexoase that could be used was limited by its low solubility and high cost, but because of its affinity for *Vh*ChiP, submillimolar concentrations of chitohexaose produced rapid swelling. In this study, we mixed chitohexaose solution with D-raffinose solution to make an isotonic solution containing 750 μM chitohexaose. The initial rate of absorbance change was monitored over the first 60 s. The swelling rate (s^{-1}) was estimated according to the equation, $\Phi = (1/A_i)dA/dt$, in which Φ is the swelling rate, A_i is the initial absorbance, and dA/dt is the rate of absorbance change during the first 60 s. The swelling rate in D-arabinose was taken as 100%, and the relative swelling rates for each sugar were compared as shown in Fig. 9, the swelling rates shown being averaged values obtained from 4–6 independent sets of experiments.

Results

Generation of VhChiP Mutants—To confirm the functional importance of Trp^{136} in ion and sugar transport, we carried out site-directed mutagenesis to evaluate the impact of this residue in regulating ion conductance, binding affinity, and sugar permeability through *Vh*ChiP. In the first set of experiments, Trp^{136} was substituted by four different amino acids with side chains having different physicochemical properties. Fig. 1 presents the top view of the *Vh*ChiP pore, depicting the original Trp side chain (Fig. 1*A*) and its substitutions with alanine (Fig. 1*B*), phenylalanine (Fig. 1*C*), arginine (Fig. 1*D*), and aspartate (Fig. 1*E*), respectively.

Purification and Confirmation of Correct Expression—After checking the nucleotide sequences of the mutagenized *ChiP* cDNAs, large scale expression trials of the recombinant *Vh*ChiP variants were performed, following the protocol established previously (9). Fig. 2*A* shows SDS-PAGE analysis of

*Vh*ChiP and its mutants after the final purification step, anion exchange chromatography. Coomassie staining showed a single band of WT *Vh*ChiP and the W136A/F/D/R mutants, migrating slightly ahead of the 40 kDa marker under denaturing conditions (reduced and heated). This corresponded to the molecular size of *Vh*ChiP expressed in *E. coli* reported previously (9, 37). Fig. 2*B* shows an immunoblot of the protein bands shown in Fig. 2*A* but detected with anti-*Vh*ChiP polyclonal antiserum. The Western blot demonstrated that the purified *Vh*ChiP WT and mutants all reacted strongly with the specific anti-*Vh*ChiP serum, whereas *E. coli* OmpN, which was often found to contaminate our recombinant *Vh*ChiP sample when the proteins were expressed in the porin-deficient *E. coli* BL21 (DE3) Omp8 Rosetta strain, was not recognized by the antibodies. The absence of cross-contamination of *Vh*ChiP with OmpN was verified using anti-OmpN polyclonal antiserum (Fig. 2*C*). This antiserum recognized the fraction containing OmpN but did not cross-react with the *Vh*ChiP preparation, indicating that all of our purified *Vh*ChiP fractions were free of OmpN and therefore suitable for functional characterization in single channel reconstitution experiments.

Effects of the Trp^{136} Mutations on the Ion Conductivity—We recently reported that a single channel of the WT *Vh*ChiP consists of three identical subunits, and, when reconstituted into phospholipid membrane, the fully open channel could conduct ions with a conductance estimated to be 1.8 ± 0.3 nS (10). In our first series of BLM experiments, we investigated the effects of Trp^{136} mutations on the ion conductivity of the *Vh*ChiP channel. Single trimeric wild-type and mutant channels were reconstituted into solvent-free membranes. Fig. 3 shows typical ion current traces, acquired over 60 s. The WT channel (Fig. 3*A*) was found to remain open almost constantly for several hours with applied transmembrane potentials of ±25 to ±150 mV. On the other hand, the mutated channels tended to exhibit frequent gating, especially with applied potentials greater than 100 mV. However, all of the mutated channels remained open for a period of several min at applied potentials of ±100 mV (Fig. 3, *B–E*), making it possible to carry out titration experiments with chitooligosaccharides. In a further series of experiments, we performed single channel recordings in solvent-containing membranes as shown in Fig. 3, *F–J* (*right*). In these membranes, a large fraction of the channels tended to be closed. Table 2 summarizes the results. In solvent-depleted membranes, the conductance of the wild-type channel was estimated to be 1.9 ± 0.02 nS, consistent with the value reported previously by Suginta *et al.* (9). The ion conductance was found to be significantly increased in the mutants W136A (2.2 ± 0.05 nS) and W136D (2.3 ± 0.03 nS) but slightly decreased in W136F (1.9 ± 0.02 nS) and significantly decreased in W136R (1.7 ± 0.02 nS). Similar results were observed with the solvent-containing membranes and different electrolytes. The results suggested that mutations of Trp^{136} had comparable effects on ion conductance of *Vh*ChiP. In addition, the phosphate buffer used in these experiments (see "Experimental Procedures") appeared to affect the ion conductance, but overall, it did not alter the pattern of relative conductance changes in the Trp^{136} mutations. In Table 2, the three conductance values reported for WT *Vh*ChiP (1.7, 1.1, and 0.6 ns) and for mutants W136A (2.5, 1.5, and 1.8 ns) and W136F (1.8, 1.2, and 0.6 ns) correspond to the opening of three, two, or one channels within the trimer; only two conductance values were obtained for mutants W136F/D (2.4 and 0.8 nS) and W136R (1.6 and 0.6 nS). The largest values presumably correspond to the opening of all three channels within the trimeric protein, whereas the two-thirds and one-third values relate to two and one openings, respectively.

Effects of the Trp^{136} Mutations on Binding Affinity, Measured by Time-resolved BLM Measurements—Titration of a single trimeric *Vh*ChiP with chitohexaose in the concentration range 0–5 μM revealed concentration-dependent channel blockages. Fig. 4 shows 500-ms-long ion current recordings of the *Vh*ChiP variants with the addition of chitohexaose on the *cis* side and an applied potential of +100 mV. The pattern of sugar-blocking events in the WT channel (Fig. 4*A*) was compared with those observed with the mutant channels W136A (Fig. 4*B*), W136F (Fig. 4*C*), W136R (Fig. 4*D*), and W136D (Fig. 4*E*). Single point mutations of Trp^{136} were found to increase both the on-rate and the off-rate of chitohexaose binding, but the greater effect was on the off-rate. The off-rates for W136A and W136R were 20-fold greater than that of the wild-type, indicating that the sugar entered and left the mutant channels much more quickly than the WT channel. Furthermore, the sugar blocking events were observed to be much more irregular, indicating incomplete subunit blocking. Our previous report showed that chitohexaose at a very low concentration (0.25 μM) usually blocked one protein monomer and occasionally blocked a second. In the

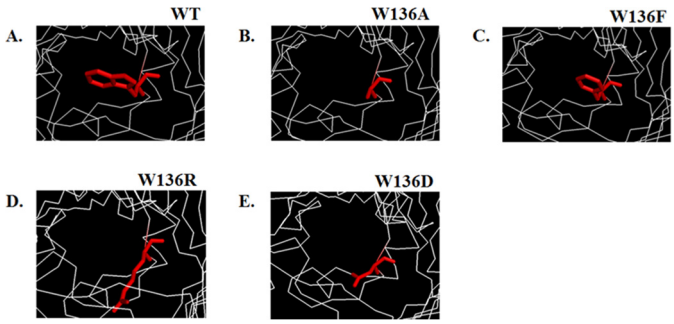

FIGURE 1. **Structures of the monomeric WT *Vh*ChiP from *V. harveyi* (*A*) and mutants W136A (*B*), W136F (*C*), W136R (*D*), and W136D (*E*).** The structures of *Vh*ChiP and its mutants were modeled using the x-ray structure of *C. acidovorans* Omp32 (Protein Data Bank entry 1E54) (20) as a template.

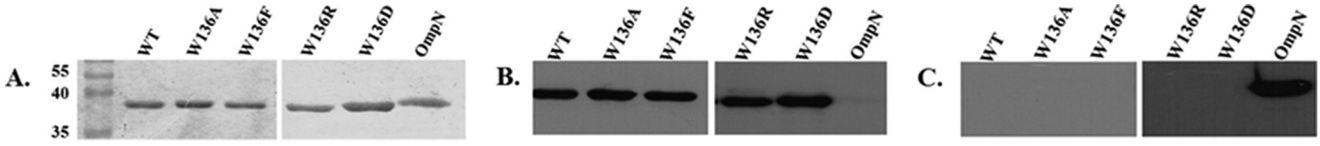

FIGURE 2. **Protein expression, purification, and immunoblotting analysis of WT and its mutants.** *A*, SDS-PAGE analysis of purified WT and its mutants, after isopropyl β-D-thiogalactoside-induced expression for 6 h. The proteins were extracted with 2% SDS, followed with 3% *n*-octylpolyoxyethylene, and further purified using Hi-Trap Q column chromatography. Immunoblotting detected with anti-*Vh*ChiP (*B*) and anti-OmpN (*C*) polyclonal antibodies.

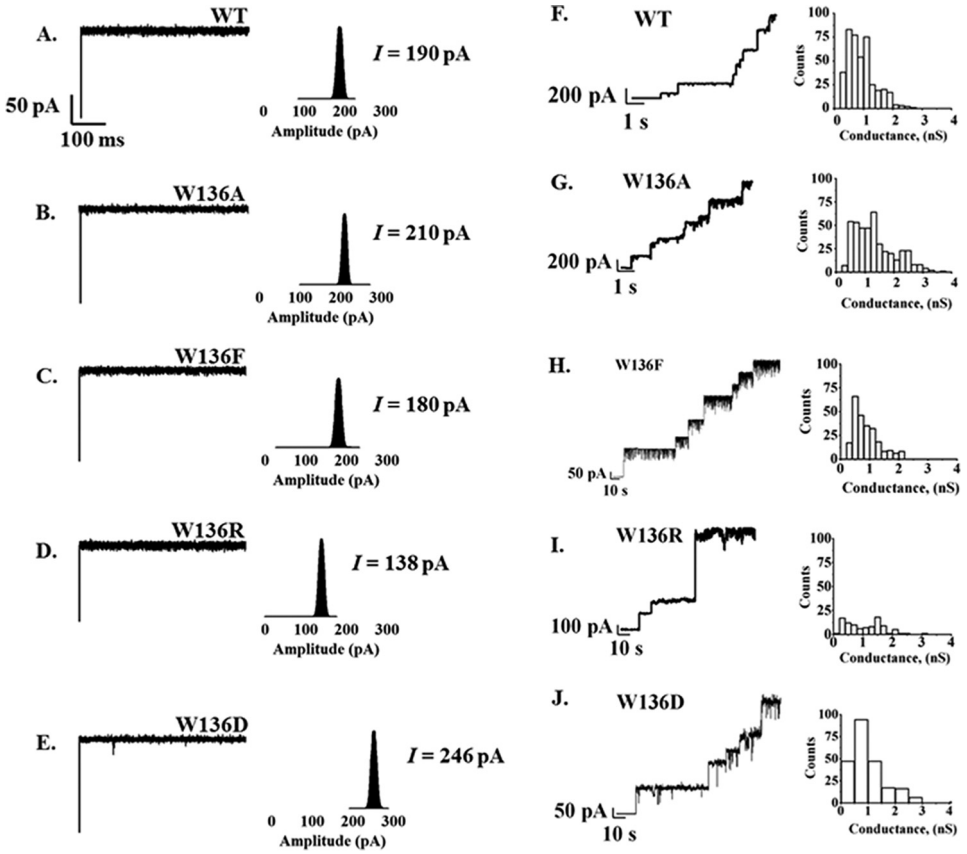

FIGURE 3. **Single channel insertion of 1,2-diphytanoyl-*sn*-glycero-3-phosphatidylcholine-bilayer membrane in the presence of WT and its mutants.** *Left*, BLM measurements using solvent-free membranes. Single channel recordings and the histogram represent the fully open state of WT (*A*) and mutants W136A/F/R/D (*B–E*) at a transmembrane potential of +100 mV. *Right*, the stepwise insertion of WT (*F*) and the same series of mutants (*G–J*) in solvent-containing 1,2-diphytanoyl-*sn*-glycero-3-phosphatidylcholine-bilayer membrane, with their corresponding histograms representing average conductance at +100 mV. The bulk solution was 1 M KCl in 20 mM HEPES, pH 7.5, and 50–100 μg of protein was added.

TABLE 2

Single channel conductance of *Vh*ChiP wild-type and mutants, as determined by two different BLM techniques

The membranes were formed by dissolving 1,2-diphytanoyl-*sn*-glycero-3-phosphatidylcholine in *n*-pentane or *n*-decane. The electrolyte contained 1 M KCl in 20 mM HEPES, pH 7.5. The applied potential was −100 mV, and the BLM measurements were carried at 20 ± 3 °C. The three conductance values shown in the solvent-containing membrane BLM technique correspond to the opening of a trimeric channel. The biggest values present the opening of three channels, whereas the two-thirds and one-third values were related to two and one openings, respectively. *n* shown in parentheses represents number of channels that were used for calculating ion conductance.

	Conductance (*G*)				
1 M KCl (20 mM HEPES, pH 7.5)	Wild type	W136A	W136F	W136D	W136R
			nS		
Solvent-depleted membrane	1.9 ± 0.03 (17)	2.2 ± 0.05 (16)	1.9 ± 0.02 (18)	2.3 ± 0.03 (22)	1.7 ± 0.02 (12)
Solvent-containing membrane	1.7 ± 0.30 (79)	2.5 ± 0.33 (80)	1.8 ± 0.33 (27)	2.4 ± 0.52 (22)	1.6 ± 0.35 (45)
	1.1 ± 0.08 (101)	1.5 ± 0.23 (116)	1.2 ± 0.22 (48)		
	0.6 ± 0.17 (238)	0.8 ± 0.27 (230)	0.6 ± 0.21 (150)	0.8 ± 0.43 (206)	0.6 ± 0.25 (52)

case of the Trp[136] mutants, only one channel subunit of the mutants W136A/F/D/R was partially blocked. At a high concentration (5.0 μM) of chitohexaose, monomeric, dimeric, and even trimeric blockages occurred in the case of WT *Vh*ChiP (Fig. 4*A*) and the W136F mutant (Fig. 4*D*), whereas at the same sugar concentration, only one subunit of the mutant W136A (Fig. 4*B*) was blocked, and dimeric blockages were infrequently seen with the W136R (Fig. 4*C*) and W136D (Fig. 4*E*) mutants.

Fig. 5 shows the effect of chitohexaose on the *Vh*ChiP channel with respect to time constants for closing (τ_c) and opening (τ_o). Note that τ_c is referred to the residence or dwell time for sugar blockage. For the WT channel, increasing concentrations of chitohexaose caused only slight changes in τ_c, the values lying within the S.D. τ_c is expected to be concentration-independent and therefore constant over the entire range of concentration (Fig. 5*A*). Mutations of Trp[136] caused a drastic reduction in τ_c over the entire range of the sugar concentration. At 2.5 μM, τ_c decreased in the following order: WT (6.7 ms) > W136F (2.3 ms) > W136D (0.5 ms) > W136R (0.34 ms) > W136A (0.32 ms). Because τ_c is the inverse of k_{off} (see Equation 2), large increases in k_{off} were observed (Table 3). Taking *cis* side addition and −100 mV applied potential as a representative example, k_{off} for the Ala and Arg mutants was 20-fold greater and, for the Asp mutant, 13-fold greater than k_{off} for the wild type. In contrast, the value of τ_o exhibited a strong concentration dependence and decreased sharply as the concentration of chitohexaose increased. As seen in Fig. 5*B*, the various mutations had only a small effect on τ_o, the on-rates for the mutated channels

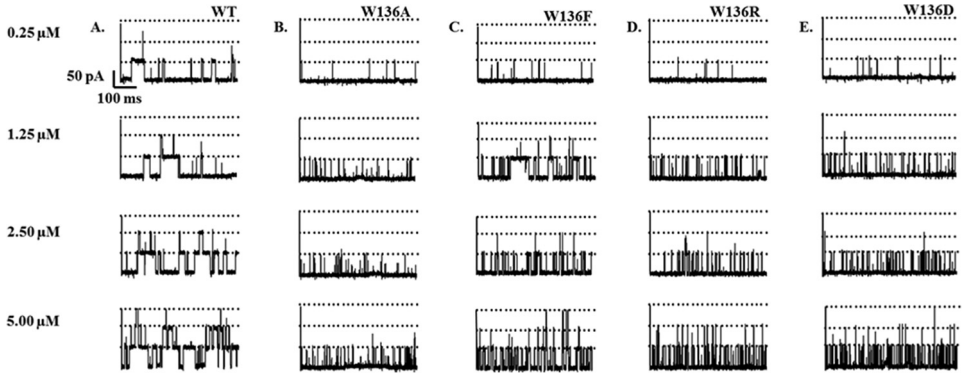

FIGURE 4. **Effect of transmembrane potentials at various concentrations of chitohexaose on the single channel insertion of *Vh*ChiP WT and its Trp[136] mutants.** Single channel insertion of WT (*A*) and mutants W136A/F/R/D (*B–E*) was reconstituted into a solvent-free lipid membrane, containing 1 M KCl in 20 mM HEPES, pH 7.5. Various concentrations of chitohexaose (0.25, 1.25, 2.5, and 5 μM) was added to the *cis* side of the membrane. The data were recorded at a transmembrane potential of −100 mV.

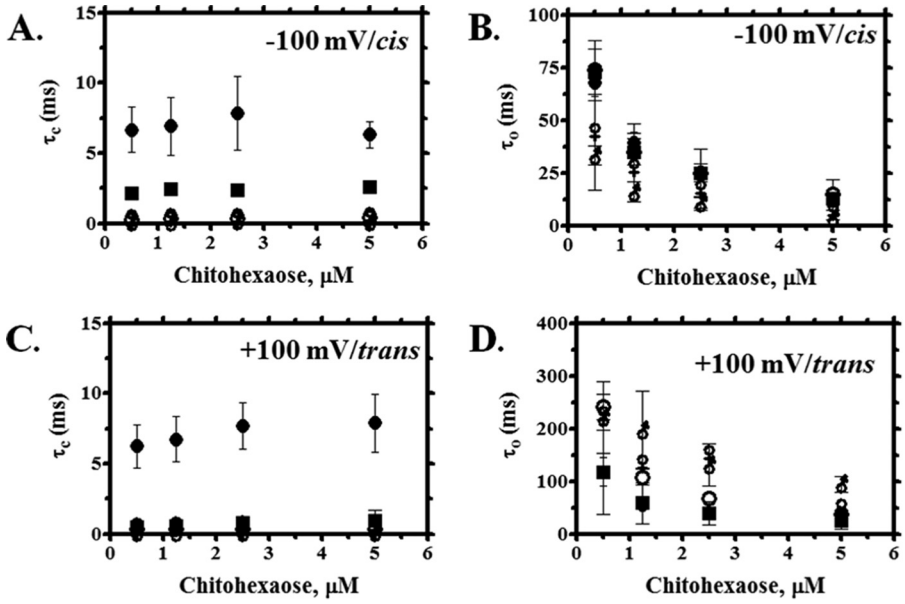

FIGURE 5. **Analysis of ion current blockades at *cis*/−100 mV or *trans*/+100 mV side addition of chitohexaose on the single channel insertion of WT and its mutant.** Shown is a plot of residence (dwell) time (τ_c) (*A* and *C*) and open time (τ_o) (*B* and *D*) *versus* various concentrations of chitohexaose. ●, WT; ○, W136A; ■, W136F; ♀, W136R; ☼, W136D. *Error bars*, S.D.

TABLE 3

Comparison of the rates and the equilibrium of binding constants (*K*, M^{-1}) of *Vh*ChiP WT and mutants for chitohexaose

The equilibrium binding constant (*K*, M^{-1}) is estimated from Equation 1, which is derived from the relative reduction of the average single channel conductance when the channel is titrated with different concentrations of chitohexaose. The on-rate (k_{on}, $M^{-1}\cdot s^{-1}$) is given by $k_{on} = K\cdot k_{off}$, and the off-rate (k_{off}, s^{-1}) is from the single trimeric molecule of *Vh*ChiP channel and its mutant after titration with different concentrations of chitohexaose that was obtained from $k_{off} = 1/\tau_c$.

*Vh*ChiP variant	*Cis*-side addition						*Trans*-side addition					
	+100 mV			−100 mV			+100 mV			−100 mV		
	$k_{on}\cdot10^6$	$k_{off}\cdot10^3$	*K*	$k_{on}\cdot10^6$	$k_{off}\cdot10^3$	*K*	$k_{on}\cdot10^6$	$k_{off}\cdot10^3$	*K*	$k_{on}\cdot10^6$	$k_{off}\cdot10^3$	*K*
	$M^{-1}\cdot s^{-1}$	s^{-1}	M^{-1}	$M^{-1}\cdot s^{-1}$	s^{-1}	M^{-1}	$M^{-1}\cdot s^{-1}$	s^{-1}	M^{-1}	$M^{-1}\cdot s^{-1}$	s^{-1}	M^{-1}
WT	55	0.25	220,000 ± 50,000	105	0.15	700,000 ± 297,000	63	0.15	420,000 ± 190,000	46	0.2	230,000 ± 14,000
W136A	500	5	100,000 ± 68,000	500	3.12	160,000 ± 38,000	760	3.3	230,000 ± 15,000	504	3.6	140,000 ± 5,000
W136F	544	1.7	320,000 ± 3,000	142	0.43	330,000 ± 45,000	495	1.5	330,000 ± 3,500	510	3.4	150,000 ± 2,000
W136R	540	2	270,000 ± 19,000	1,110	3	370,000 ± 4,500	153	1.7	90,000 ± 4,500	175	2.5	70,000 ± 8,500
W136D	308	7.7	40,000 ± 2,500	200	2	100,000 ± 850	693	7.7	90,000 ± 1,900	250	6.25	40,000 ± 1,300

being less affected than the off-rates (Table 3). Similar effects were observed with the *trans* addition of sugars at an applied voltage of +100 mV, all mutants showing significantly decreased values of τ_c (Fig. 5*C*) but a lesser decrease in τ_o (Fig. 5*D*).

Fig. 6 shows the binding isotherms for the individual *Vh*ChiP mutant channels, with relative conductance changes plotted as a function of the chitohexaose concentration on the *cis* side at −100 mV (Fig. 6*A*). Fitting curves using a nonlinear regression function yielded hyperbolic plots, and these non-linear plots were converted to Lineweaver-Burk plots (Fig. 6*B*), allowing the binding constants to be estimated directly.

Consistent results were observed with chitohexaose added on the *trans* side at an applied potential of +100 mV. Fig. 6, *C*

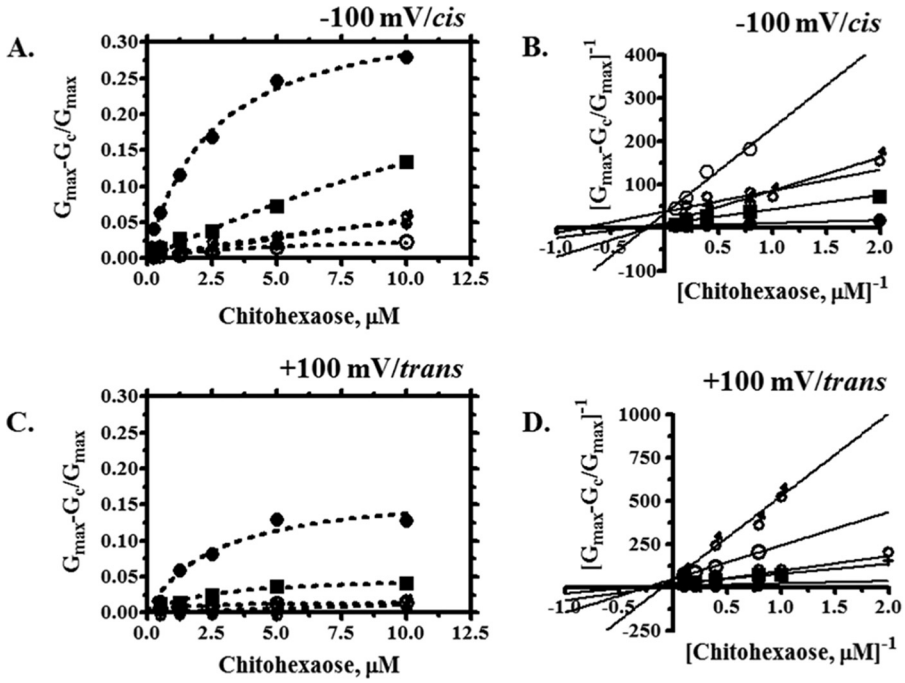

FIGURE 6. **Binding curve and Lineweaver-Burk plots of WT and its mutant with chitohexaose.** The Michaelis-Menten plots were obtained from the data on the *cis*/−100 mV (*A*) or *trans*/+100 mV (*C*) side addition. The plot of $(G_{max} - G_c)/G_{max}$ *versus* various concentrations of chitohexaose (0.25–10 μM) were derived from Equation 2. Lineweaver-Burk plots of WT and its mutant were obtained from the various concentrations of chitohexaose (0.25–10 μM), at −100 mV/*cis* (*B*) or +100 mV/*trans* (*D*) side addition. ●, WT; ○, W136A; ■, W136F; ♀, W136R; ✧, W136D.

and *D*, shows the non-linear binding plots and their corresponding linear transformations. Decreased *K* values for all the mutants indicated that the Trp[136] mutations lower the affinity for chitohexaose. With all mutants, binding increased proportionally with increasing concentration of the sugar and did not reach saturation within the selected concentration range. The greatest reduction in the stability constant for sugar binding was observed with the mutant W136A, whereas the smallest effect was found with the W136F mutant. The binding affinity (*K*) of each *Vh*ChiP mutant for chitohexaose was estimated from the Lineweaver-Burk plot of the titration data.

Table 3 summarizes the kinetic values (k_{on}, k_{off}, and *K*) obtained from the binding curves shown in Fig. 6 under different experimental conditions. The BLM data were acquired under four different regimes: with sugar addition on the *cis* side or the *trans* side and an applied potential of −100 or +100 mV. The largest k_{on} and *K* and smallest k_{off} were observed with *cis* addition at −100 mV. Different conditions produced different kinetic values, confirming the asymmetric properties of the *Vh*ChiP channel. The *K* values of the WT channel obtained under the conditions of highest activity, *cis* addition/−100 mV and *trans* addition/+100 mV (700,000 M^{-1} and 420,000 M^{-1}), were close to the values (500,000 and 370,000 M^{-1}) reported previously (10).

Under the condition *cis* addition/−100 mV, the mutants W136D and W236A showed a large decrease in the binding constants, relative to the WT channel, with 7- and 4-fold lower values for *K*, respectively. Other mutants, including W136F and W136R, also showed reduced affinity, their *K* values being about 2-fold less than that for WT *Vh*ChiP. Similar trends were observed under the condition *cis* addition/+100 mV. With *trans* addition of substrate, at both applied potentials (±100 mV), there were very large decreases in *K* for the mutants W136D and W136R, whereas the mutants W136A and W136F showed only a moderate reduction. It is interesting to note that the Trp[136] mutations considerably affected chitohexaose binding by increasing both the on-rates and the off-rates, but the effect on the off-rates was generally greater than on the on-rates. For example, k_{off} for W136A was increased by a factor of about 20 as compared with k_{off} of WT, whereas k_{on} of W136A was increased only about 5-fold.

Effects of Trp[136] Mutation on the Binding Affinity Revealed by Fluorescence Spectroscopy—Intrinsic fluorescence changes were used to assess the binding affinity of *Vh*ChiP and its mutants for chitooligosaccharides. We first counted the number of Trp residues in the amino acid sequence of WT *Vh*ChiP. Fig. 7*A* shows that it contained 10 Trp residues (underlined) at positions 73, 105, 123, 136, 155, 185, 216, 228, 268, and 331. Three of these may be located inside the channel: Trp[136] extends into the center, whereas Trp[123] and Trp[228] protrude from the inner wall in the lower part of the protein lumen (Fig. 7*B*). Trp[216] and Trp[331] are parts of the extracellular loops L5 and L8 and lie on the outside of the pore. Other tryptophan residues are located at different positions around the outer surface of the β-barrel. The Trp[136] mutations generally affected the intrinsic fluorescence properties of the protein (Fig. 7*C*). In the absence of ligand, the mutants W136A and W136D showed a large reduction in the fluorescence intensity, as compared with that of the WT channel, whereas W136R showed a moderate decrease. The largest influence on the intrinsic fluorescence was seen in the mutant W136F, which showed a significant increase in the fluorescence

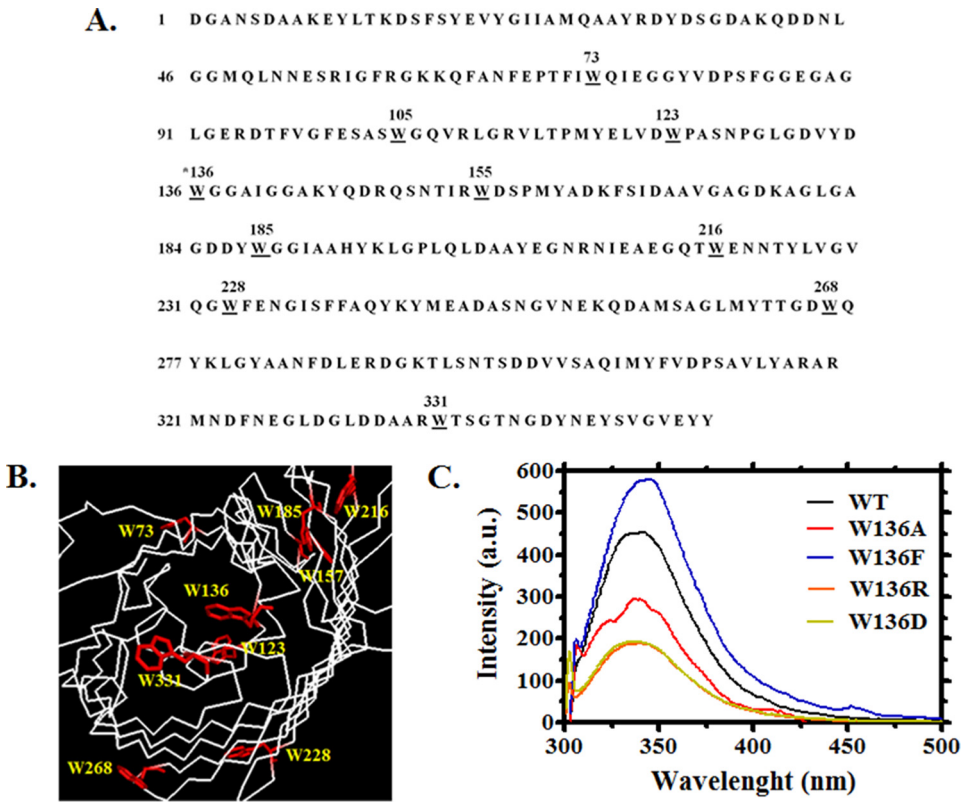

FIGURE 7. **Amino acid sequence and cross-section of the prospective three-dimensional structure of monomeric chitoporin from *V. harveyi*.** *A*, amino acid sequence of *Vh*ChiP with all tryptophan residues *underlined*. *B*, amino acid residues that may be important for ion and sugar passages through the constriction zone of the *Vh*ChiP channel. *C*, example of the emission spectra from *Vh*ChiP WT and its Trp[136] mutants, showing changes in fluorescence intensity caused by Trp[136] mutations. The emission spectra were acquired at wavelengths between 300 and 550 nm using an excitation wavelength of 295 nm. The protein concentration used was 40 ng·μl^{-1} in 20 mM potassium phosphate buffer, pH 7.4, containing 0.2% (v/v) LDAO.

intensity and a shift of its wavelength of maximum emission from 340 to 350 nm.

Each *Vh*ChiP mutant was titrated with chitohexaose, and the plots of Trp fluorescence quenching or enhancement were compared with the titration of WT protein (Fig. 8, *A–E*, *top panels*). Chitohexaose decreases the fluorescence intensity of WT *Vh*ChiP in a concentration-dependent manner, whereas in the mutants W136F, W136D, and W136R, chitohexaose enhances the fluorescence signal, at much higher concentrations. Plots of relative changes in fluorescence intensity as a function of chitohexaose concentrations yielded binding curves similar to the binding curves obtained with chitohexaose titration of single channels reconstituted into BLM. Fitting of the binding curve for each *Vh*ChiP homolog was performed using non-linear regression (Fig. 8, *A–E*, *left panels*). For the mutant W136A, data fitting did not provide reliable parameter values, because titration of this mutant with chitohexaose did not significantly change the fluorescence intensity, indicating weak interaction between the sugar and the protein (Fig. 8*B*).

Curve fitting of the fluorescence intensity plotted against sugar concentration yielded the binding constants *K*, summarized in Table 4. The relative values of *K* determined by fluorescence titration were consistent with those obtained from BLM measurements, although the absolute values differed. This discrepancy might have many origins, considering the different environment of the *Vh*ChiP in the different types of experiment; fluorescence titration was performed with the detergent-solubilized channels, rather than with channels reconstituted in lipid bilayers, and there was no trans-channel potential. Moreover, fluorescence counts all Trp and not only those located in the channel constriction. Mutants W136A, W136D, and W136R showed a large reduction in *K*, indicating reduced binding affinity, especially in mutant W136D, for which the binding constant was 20-fold lower than that of WT. In mutants W136A and W136R, the binding affinity was reduced to about the same extent, with a 12- and 10-fold decrease in *K*, respectively, whereas mutant W136F showed only slightly decreased affinity, with *K* being 2.8-fold lower than in the wild type.

Effects of Trp[136] Mutation on Sugar Permeation, Measured by a Liposome Swelling Assay—To further study the effect of Trp[136] mutations on sugar permeability, liposome swelling assays were performed. As shown in Fig. 9, the relative swelling rates, which reflect the rates of permeation by chitohexaose, were compared with the rate of swelling in isotonic solution of the permeant sugar arabinose, which was taken as 100%, whereas an isotonic solution of the impermeant sugar raffinose served as a control. At a fixed chitohexaose concentration of 750 μM, the relative permeability of WT *Vh*ChiP (14 ± 6.5%) was greater than that of all of the mutant forms of the channel. W136A showed the lowest permeability (2 ± 1.3%), followed by W136R (3 ± 1.1%), W136D (5 ± 2.8%), and W136F (8 ± 2.1%).

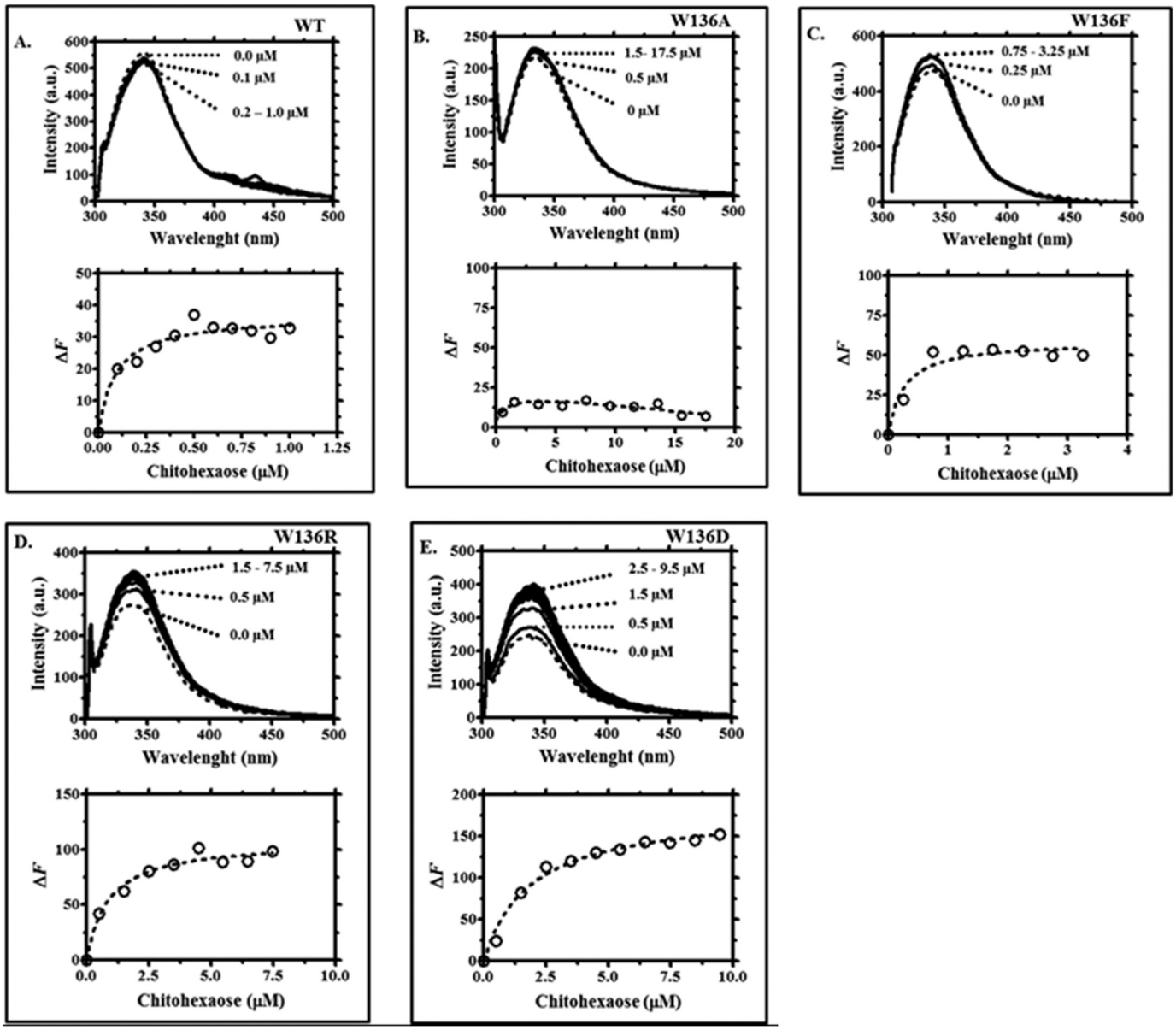

FIGURE 8. **Tryptophan quenching fluorescence spectra of *Vh*ChiP WT (*A*) and mutants W136A/F/R/D (*B–E*).** *Top*, the titration curves, showing changes in the fluorescence intensity with increasing concentrations of chitohexaose added to the protein solution. Bottom, curve fits of the nonlinear transformation of the above titration curves.

TABLE 4

Determination of the equilibrium binding constant (*K*) of *Vh*ChiP WT and its mutants with chitohexaose from the non-linear curve fit shown in Fig. 8, following Equation 5

Ligand	*Vh*ChiP variant	*K*
		M^{-1}
Chitohexaose	WT	11,000,000 ± 350,000
	W136A	909,000 ± 16,500
	W136F	4,000,000 ± 130,000
	W136D	530,000 ± 20,000
	W136R	1,150,000 ± 250,000

Discussion

Chitoporin (*Vh*ChiP) from the marine bacterium *V. harveyi* was recently identified as a channel that is able to transport the degradation products of chitin, with a high selectivity for chitohexaose (10). Although chitoporin is a sugar-specific channel isolated from the outer membrane of Gram-negative bacteria, this channel shows only low sequence identity to other channels of known carbohydrate specificity, such as LamB or ScrY (12, 13). The residues identified as the aromatic track in maltoporin (LamB) or sucrose porin (ScrY) were not found in chitoporin. Moreover, our functional investigation revealed that *Vh*ChiP does not interact with maltooligosaccharides. Therefore, *Vh*ChiP and LamB are likely to have quite different structures facilitating sugar passage.

Our structure of *Vh*ChiP, derived from the three-dimensional structure of Omp32 (20, 38), shows that Trp^{136} is part of the longest loop (L3) that protrudes into the channel lumen. This residue is located prominently in the center of the pore, covering the entrance of the constriction zone. Therefore, this residue is presumed to be crucial for controlling ion flow and to affect binding affinity and sugar permeation through the *Vh*ChiP channel. Trp^{136} was mutated to Ala, Phe, Asp, and Arg,

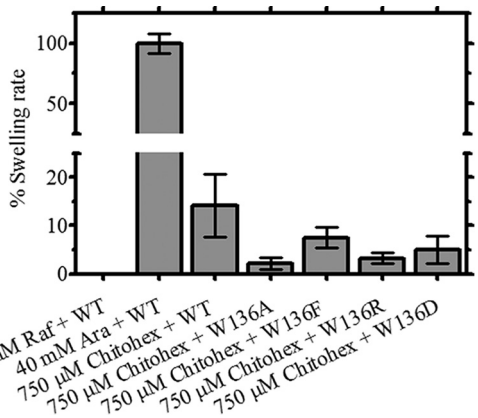

FIGURE 9. **Results of the liposome swelling assays.** Multilamellar liposomes, prepared as described under "Experimental Procedures," were reconstituted with purified *Vh*ChiP and its mutants. The isotonic concentration was defined as the concentration of raffinose added into the proteoliposome suspension that did not cause an absorbance change at 500 nm for a period of 60 s. Permeation of different types of sugars through the *Vh*ChiP-reconstituted liposomes was tested. Their swelling rates were normalized to the rate of arabinose, set to 100%. Bar graphs show average values ± S.D. (*error bars*) obtained from the experiments carried in triplicate.

so as to generate a series of Trp[136] mutants with different physicochemical properties. According to standard scales of hydrophobicity (39), the side chain of Ala is small and neutral, whereas Phe has increased aromaticity and hydrophobicity. The Asp side chain is acidic and thus negatively charged, whereas the Arg side chain is highly basic and therefore positively charged.

Mutation of Trp[136] to Ala considerably increased ion flow, resulting in the larger conductance of the mutant W136A. The explanation is clear; the substitution of Trp[136] by Ala removed the steric hindrance caused by the bulky side chain of Trp. In contrast, the single channel conductance of the W136F mutant was not much changed from the WT conductance, indicating that the Phe side chain had a steric effect similar to that of Trp and that ion flow through the *Vh*ChiP channel was not greatly influenced by the different degree of hydrophobicity. That mutation of the pore-lining residues leads to modified ion flux was demonstrated previously in maltoporin (LamB) and sucrose porin. Orlik *et al.* (11) reported changes in the channel conductance when Tyr[118], located in the constriction zone of the LamB channel, was mutated to various amino acids. The largest conductance change was observed with Ala (850 pS) and Asp (1,050 pS) substitution and resulted in conductance that was ~5- and 7-fold larger, respectively, than that of the native channel (155 pS). Moreover, substitutions of residues within the polar track also greatly decreased the rate of sugar transport, compared with the wild-type LamB (30). Similarly, single mutants (D201Y, N192R, and F204D), generated by mutation of the central constriction residues of the sucrose porin (ScrY), showed decreased channel conductance as well as narrowing the sucrose passage of this channel (40, 41).

We further measured the K^+/Cl^- selectivity of the wild-type channel, which showed a preference for cations ($P_c/P_a = 3.2$). The mutant W136D exhibited increased ion conductance, which is expected for a channel with cation selectivity, because mutation of Trp to a negatively charged residue should increase the selectivity of the channel for cations (42). Conversely, the substitution of Trp[136] with Arg reduced the ion conductance from 1.9 to 1.7 nS (Table 2), the switch to a positively charged side chain inhibiting cation flux. Selectivity for cations over anions was also seen with LamB and OmpF (11). The LamB channel has more pronounced cationic selectivity than *Vh*ChiP, with a P_c/P_a ratio of about 5.5, whereas that for OmpF was about 5.0. Shifts of ion selectivity when different charged residues were introduced into the pore lumen clearly indicated that the ionization states of residues in the pore interior are crucial for regulating ion transport through the *Vh*ChiP channel.

The effects of Trp[136] mutations on the binding affinity of *Vh*ChiP were subsequently investigated by titrating single, fully open mutated channels with chitohexaose, at concentrations up to 10 μM. Time-resolved current measurements showed that the sugar transiently blocked the ion flow, although the blocking behavior was quite different from that of the WT channel. With WT *Vh*ChiP, the number of blocking events increased linearly with increasing concentration of chitohexaose up to 2.5 μM and then reached a plateau, with no further increase at concentrations of 5 μM or higher, suggesting that the channel was saturated even at a low concentration of the sugar, due to the high affinity of chitohexaose binding. It is important to note that the observed *K* values presented in Table 3 were affected to various extents by applied external potentials and by the side of sugar addition. The results reflect highly dynamic as well as asymmetric features of the *Vh*ChiP channel as noted in our previous study (10). Current fluctuations that gave rise to changes in average conductance were also affected by the inherent behaviors of individual channels.

Analyzing the ion current fluctuations with respect to residence (dwell) times (τ_c), the sugar molecules were found to stay in the modified pores for a shorter time, indicated by a decrease in their residence times, compared with WT. Large changes were observed with mutants W136A, W136D, and W136R, whereas mutant W136F showed only a slight change in the residence time. These results again confirmed that the steric properties of the aromatic side chain of the mutated residue play a prominent role in maintaining intrinsic affinity of binding between the sugar substrate and the channel interior.

All mutants showed significant decreases in the value of the binding constant, *K*, as a result of effects on both the on-rate and the off-rate. Increases in the on-rate indicate faster entry of the *Vh*ChiP pore by chitohexaose, whereas increases in the off-rate indicate that the interacting sugar molecules leave the channel more quickly. However, the dominant effects were on the off-rate constant, especially with the W136A and W136D mutants. In these cases, k_{off} was increased up to 20-fold over k_{off} for the wild-type channel. Such results suggest that the Ala and Asp substitutions of Trp[136] decrease the affinity of binding by accelerating the dissociation of the sugar molecule from the channel lumen and thus increasing the turnover number. Likewise, Trp[136] mutation also altered bulk sugar permeability through the *Vh*ChiP channel. This conclusion was supported by the results from liposome swelling assays, which showed a considerable reduction in the rate of chitohexaose permeation through all of the mutated channels. Consistent with the BLM measurements, the effects were clearly observed with W136A,

W136R, and W136D mutants. In summary, our data provide evidence that the residue Trp^{136} plays a significant role in controlling the ion conductivity, sugar binding affinity, and sugar permeability of this highly potent chitooligosaccharide-specific channel.

Conclusion

Chitoporin is a sugar-specific channel strictly required by *Vibrios* for nutrient uptake. Our studies help to shed light on the mechanism of chitin uptake through the outer membrane of these bacteria. Crucially, understanding the mechanistic details of chitin transport through chitoporin should pave the way for the design of novel specific channel blockers that offer an effective strategy to control the epidemic of fatal diseases caused by *Vibrios*, such as vibriosis by *V. harveyi*, which causes a vast economic loss in farmed shrimp and fish industries worldwide, or cholera by *Vibrio cholerae*, which, according to a World Health Organization report (43), causes 100,000–120,000 deaths annually.

Author Contributions—W. C. designed, performed, and analyzed all of the experiments presented in this paper. M. W. and R. B. provided expertise on BLM experiments and data analysis and prepared and approved the final draft of the paper. A. S. provided technical assistance and contributed to the preparation of the manuscript. W. S. conceived and coordinated the study, provided advice on the liposome swelling assay and fluorescence binding measurements, and wrote and revised the paper. All authors reviewed the results and approved the final version of the manuscript.

Acknowledgments—We acknowledge the Biochemistry Laboratory, Center for Scientific and Technological Equipment, Suranaree University of Technology for providing all research facilities. We greatly appreciate a critical reading of the manuscript by Dr. David Apps (Centre for Integrative Physiology, School of Biomedical Sciences, University of Edinburgh, UK).

REFERENCES

1. Abraham, T. J., and Palaniappan, R. (2004) Distribution of luminous bacteria in semi-intensive penaeid shrimp hatcheries of Tamil Nadu, India. *Aquaculture* **232,** 81–90
2. Haldar, S., Maharajan, A., Chatterjee, S., Hunter, S. A., Chowdhury, N., Hinenoya, A., Asakura, M., and Yamasaki, S. (2010) Identification of *Vibrio harveyi* as a causativebacterium for a tail rot disease of sea bream *Sparus aurata* from research hatchery in Malta. *Microbiol. Res.* **165,** 639–648
3. Ransangan, J., and Mustafa, S. (2009) Identification of *Vibrio harveyi* isolated from diseased Asian Seabass *Lates calcarifer* by use of 16S ribosomal DNA sequencing. *J. Aquat. Anim. Health* **21,** 150–155
4. Tendencia, E. A. (2002) *Vibrio harveyi* isolated from cage-cultured seabass *Lates calcarifer Bloch* in the Philippines. *Aquacult. Res.* **33,** 455–458
5. Vezzulli, L., Previati, M., Pruzzo, C., Marchese, A., Bourne, D. G., Cerrano, C., and VibrioSea Consortium (2010) *Vibrio* infections triggering mass mortality events in a warming Mediterranean Sea. *Environ. Microbiol.* **12,** 2007–2019
6. Jung, B. O., Roseman, S., and Park, J. K. (2008) The central concept for chitin catabolic cascade in marine bacterium, *Vibrios*. *Macromol. Res.* 10.1007/BF03218953
7. Hunt, D. E., Gevers, D., Vahora, N. M., and Polz, M. F. (2008) Conservation of the chitin utilization pathway in the *Vibrionaceae*. *Appl. Environ. Microbiol.* **74,** 44–51
8. Bassler, B. L., Yu, C., Lee, Y. C., and Roseman, S. (1991) Chitin utilization by marine bacteria: degradation and catabolism of chitin oligo-saccharides by *Vibrio furnissii*. *J. Biol. Chem.* **266,** 24276–24286
9. Suginta, W., Chumjan, W., Mahendran, K. R., Janning, P., Schulte, A., and Winterhalter, M. (2013) Molecular uptake of chitooligosaccharides through chitoporin from the marine bacterium *Vibrio harveyi*. *PLoS One* **8,** e55126
10. Suginta, W., Chumjan, W., Mahendran, K. R., Schulte, A., and Winterhalter, M. (2013) Chitoporin from *Vibrio harveyi*: a channel with exceptional sugar specificity. *J. Biol. Chem.* **288,** 11038–11046
11. Orlik, F., Andersen, C., and Benz, R. (2002) Site-directed mutagenesis of tyrosine 118 within the central constriction site of the LamB (Maltoporin) channel of *Escherichia coli.* I. Effect on ion transport. *Biophys. J.* **82,** 2466–2475
12. Andersen, C., Cseh, R., Schülein, K., and Benz, R. (1998) Study of sugar binding to the sucrose-specific ScrY channel of enteric bacteria using current noise analysis. *J. Membr. Biol.* **164,** 263–274
13. Andersen, C., Jordy, M., and Benz, R. (1995) Evaluation of the rate constants of sugar transport through maltoporin (LamB) of *E. coli* from the sugar-induced current noise. *J. Gen. Physiol.* **105,** 385–401
14. Saravolac, E. G., Taylor, N. F., Benz, R., and Hancock, R. E. (1991) Purification of glucose-inducible outer membrane protein OprB of *Pseudomonas putida* and reconstitution of glucose-specific pores. *J. Bacteriol.* **173,** 4970–4976
15. Wylie, J. L., Bernegger-Egli, C., O'Neil, J. D., and Worobec, E. A. (1993) Biophysical characterization of OprB, a glucose-inducible porin of *Pseudomonas aeruginosa*. *J. Bioenerg. Biomembr.* **25,** 547–556
16. Pajatsch, M., Andersen, C., Mathes, A., Böck, A., Benz, R., and Engelhardt, H. (1999) Properties of a cyclodextrin-specific, unusual porin from *Klebsiella oxytoca*. *J. Biol. Chem.* **274,** 25159–25166
17. Orlik, F., Andersen, C., Danelon, C., Winterhalter, M., Pajatsch, M., Böck, A., and Benz, R. (2003) CymA of *Klebsiella oxytoca* outer membrane: binding of cyclodextrins and study of the current noise of the open channel. *Biophys. J.* **85,** 876–885
18. Hilty, C., and Winterhalter, M. (2001) Facilitated substrate transport through membrane proteins. *Phys. Rev. Lett.* **86,** 5624–5627
19. Suginta, W., and Smith, M. F. (2013) Single-molecule trapping dynamics of sugar-uptake channels in marine bacteria. *Phys. Rev. Lett.* **110,** 238102
20. Zeth, K., Diederichs, K., Welte, W., and Engelhardt, H. (2000) Crystal structure of Omp32, the anion-selective porin from *Comamonas acidovorans*, in complex with a periplasmic peptide at 2.1 Å resolution. *Structure* **8,** 981–992
21. Forst, D., Welte, W., Wacker, T., and Diederichs, K. (1998) Structure of the sucrose-specific porin ScrY from *Salmonella typhimurium* and its complex with sucrose. *Nat. Struct. Biol.* **5,** 37–46
22. Schirmer, T., Keller, T. A., Wang, Y. F., and Rosenbusch, J. P. (1995) Structural basis for sugar translocation through maltoporin channels at 3.1 Å resolution. *Science* **267,** 512–514
23. Nikaido, H. (1992) Porins and specific channels of bacterial outer membranes. *Mol. Microbiol.* **6,** 435–442
24. Prilipov, A., Phale, P. S., Van Gelder, P., Rosenbusch, J. P., and Koebnik, R. (1998) Coupling site-directed mutagenesis with high-level expression: large scale production of mutant porins from *E. coli*. *FEMS Microbiol. Lett.* **163,** 65–72
25. Aunkham, A., Schulte, A., Winterhalter, M., and Suginta, W. (2014) Porin involvement in cephalosporin and carbapenem resistance of *Burkholderia pseudomallei*. *PLoS One* **9,** e95918
26. Rosenbusch, J. P. (1974) Characterization of the major envelope protein from *Escherichia coli*: regular arrangement on the peptidoglycan and unusual dodecyl sulfate binding. *J. Biol. Chem.* **249,** 8019–8029
27. Lugtenberg, B., and Van Alphen, L. (1983) Molecular architecture and functioning of the outer membrane of *Escherichia coli* and other Gram-negative bacteria. *Biochim. Biophys. Acta* **737,** 51–115
28. Schulte, A., Ruamchan, S., Khunkaewla, P., and Suginta, W. (2009) The outer membrane protein *Vh*Omp of *Vibrio harveyi*: pore-forming properties in black lipid membranes. *J. Membr. Biol.* **230,** 101–111
29. Schwarz, G., Danelon, C., and Winterhalter, M. (2003) On translocation through a membrane channel via an internal binding site: kinetics and voltage dependence. *Biophys. J.* **84,** 2990–2998

30. Danelon, C., Brando, T., and Winterhalter, M. (2003) Probing the orientation of reconstituted maltoporin channels at the single-protein level. *J. Biol. Chem.* **278,** 35542–35551
31. Mahendran, K. R., Chimerel, C., Mach, T., and Winterhalter, M. (2009) Antibiotic translocation through membrane channels: temperature-dependent ion current fluctuation for catching the fast events. *Eur. Biophys. J.* **38,** 1141–1145
32. Benz, R., and Hancock, R. E. (1987) Mechanism of ion transport through the anion-selective channel of the *Pseudomonas aeruginosa* outer membrane. *J. Gen. Physiol.* **89,** 275–295
33. Kullman, L., Winterhalter, M., and Bezrukov, S. M. (2002) Transport of maltodextrins through maltoporin: a single-channel study. *Biophys. J.* **82,** 803–812
34. Songsiriritthigul, C., Pantoom, S., Aguda, A. H., Robinson, R. C., and Suginta, W. (2008) Crystal structures of *Vibrio harveyi* chitinase A complexed with chitooligosaccharides: implications for the catalytic mechanism. *J. Struct. Biol.* **162,** 491–499
35. Srivastava, D. B., Ethayathulla, A. S., Kumar, J., Singh, N., Sharma, S., Das, U., Srinivasan, A., and Singh, T. P. (2006) Crystal structure of a secretory signaling glycoprotein from sheep at 2.0 Å resolution. *J. Struct. Biol.* **156,** 505–516
36. Neves, P., Berkane, E., Gameiro, P., Winterhalter, M., and de Castro, B. (2005) Interaction of quinolones antibiotics and bacterial outer membrane porin OmpF. *Biophys. Chem.* **113,** 123–128
37. Luckey, M., and Nikaido, H. (1980) Specificity of diffusion channel produced by lambda phage receptor protein of *Escherichia coli*. *Proc. Natl. Acad. Sci. U.S.A.* **77,** 167–171
38. Zachariae, U., Klühspies, T., De, S., Engelhardt, H., and Zeth, K. (2006) High resolution crystal structures and molecular dynamics studies reveal substrate binding in the porin Omp32. *J. Biol. Chem.* **281,** 7413–7420
39. Eisenberg, D., Schwarz, E., Komaromy, M., and Wall, R. (1984) Analysis of membrane and surface protein sequences with the hydrophobic moment plot. *J. Mol. Biol.* **179,** 125–142
40. Ulmke, C., Kreth, J., Lengeler, J. W., Welte, W., and Schmid, K. (1999) Site-directed mutagenesis of loop L3 of sucrose porin ScrY leads to changes in substrate selectivity. *J. Bacteriol.* **181,** 1920–1923
41. Kim, B. H., Andersen, C., Kreth, J., Ulmke, C., Schmid, K., and Benz, R. (2002) Site-directed mutagenesis within the central constriction site of ScrY (sucrose-porin): effect on ion transport and comparison of maltooligosaccharide binding to LamB of *Escherichia coli*. *J. Membr. Biol.* **187,** 239–253
42. Pezeshki, S., Chimerel, C., Bessonov, A. N., Winterhalter, M., and Kleinekathöfer, U. (2009) Understanding ion conductance on a molecular level: an all-atom modeling of the bacterial porin OmpF. *Biophys. J.* **97,** 1898–1906
43. World Health Organization (1995) *Meeting on the Potential Role of New Cholera Vaccines in the Prevention and Control of Cholera Outbreaks during Acute Emergencies*, Document CDR/GPV/95.1, World Health Organization, Geneva